First $g(2^+)$ measurement on neutron-rich ^{72}Zn, and the high-velocity transient field technique for radioactive heavy-ion beams

E. Fiori,[1,*] G. Georgiev,[1,†] A. E. Stuchbery,[2] A. Jungclaus,[3] D. L. Balabanski,[4] A. Blazhev,[5] S. Cabaret,[1] E. Clément,[6] M. Danchev,[7] J. M. Daugas,[8] S. Grevy,[6] M. Hass,[9] V. Kumar,[9] J. Leske,[10] R. Lozeva,[1,‡] S. Lukyanov,[11] T. J. Mertzimekis,[12] V. Modamio,[3,§] B. Mouginot,[13] F. Nowacki,[14,15] Yu. E. Penionzhkevich,[11] L. Perrot,[13] N. Pietralla,[10] K. Sieja,[14,15] K.-H. Speidel,[16] I. Stefan,[13] C. Stodel,[6] J. C. Thomas,[6] J. Walker,[3] and K. O. Zell[5]

[1]*CSNSM, CNRS/IN2P3, Université Paris-Sud 11, UMR8609, F-91405 ORSAY-Campus, France*

[2]*Department of Nuclear Physics, Australian National University, Canberra, Australia*

[3]*Instituto de Estructura de la Materia, CSIC, E-28006 Madrid, Spain*

[4]*Institute for Nuclear Research and Nuclear Energy, Bulgarian Academy of Sciences, BG-1784 Sofia, Bulgaria*

[5]*IKP, University of Cologne, D-50937 Cologne, Germany*

[6]*Grand Accélérateur National d'Ions Lourds (GANIL), CEA/DSM-CNRS/IN2P3, Boulevard H. Becquerel, F-14076, Caen, France*

[7]*Faculty of Physics, St. Kliment Ohridski University of Sofia, 1164 Sofia, Bulgaria*

[8]*CEA, DAM, DIF, F-91297 Arpajon cedex, France*

[9]*The Weizmann Institute, Rehovot, Israel*

[10]*TU Darmstadt, Darmstadt, Germany*

[11]*JINR, Dubna, Russia*

[12]*INP, NCSR "Demokritos", GR-15310, Ag. Paraskevi/Athens, Greece*

[13]*IPN, CNRS/IN2P3, Université Paris-Sud 11, UMR8608, F-91406 ORSAY-Campus, France*

[14]*Université de Strasbourg, IPHC, 23 rue du Loess F-67037 Strasbourg, France*

[15]*CNRS/IN2P3, UMR7178, F-67037 Strasbourg, France*

[16]*Helmholtz-Institut für Strahlen- und Kernphysik, Bonn, Germany*

(Received 23 September 2011; revised manuscript received 22 February 2012; published 29 March 2012)

The high-velocity transient-field (HVTF) technique was used to measure the g factor of the 2^+ state of ^{72}Zn produced as a radioactive beam. The transient-field strength was probed at high velocity in ferromagnetic iron and gadolinium hosts using ^{76}Ge beams. The potential of the HVTF method is demonstrated and the difficulties that need to be overcome for a reliable use of the TF technique with high-Z, high-velocity radioactive beams are revealed. The polarization of K-shell vacancies at high velocity, which shows more than an order of magnitude difference between $Z = 20$ and $Z = 30$ is discussed. The g-factor measurement hints at the theoretically predicted transition in the structure of the Zn isotopes near $N = 40$.

DOI: 10.1103/PhysRevC.85.034334 PACS number(s): 21.10.Ky, 21.60.Cs, 23.20.En, 27.50.+e

I. INTRODUCTION

The neutron-rich $N = 40$ region is often discussed in relation to the competition between single-particle-based structures as observed in the $Z = 28$ Ni isotopes and the collectivity observed in the $Z = 26$ and $Z = 30$ isotopes in their immediate vicinity [1–4]. Nuclear gyromagnetic ratios, with their sensitivity to the single-particle properties of the nuclear states, can provide a sensitive probe of this interplay. Whereas the g factors of the 2^+ states of the stable Ni isotopes show predominantly single particle behavior, consistent with shell model structures [5], those of the nearby Zn and Ge isotopes [6] show a trend consistent with the Z/A rule, characteristic of collective states. Particular interest in the Zn isotopes ($Z = 30$) arises from a number of theoretical calculations [7–9] which predict a change in the structure of the Zn isotopes around $N = 40$. However these calculations, which differ in the size of the basis space and the nucleon-nucleon interactions employed, make very different predictions for the strength of this transition and how sudden or gradual it might be. The g factor of the last stable isotope ^{70}Zn does not deviate strongly from Z/A. In this work we seek to extend the g-factor data to neutron-rich ^{72}Zn where, according to some of the theoretical calculations (e.g., Ref. [9]), a strong deviation of the g factor from the hydrodynamical limit might occur.

Gyromagnetic-ratio measurements on excited states of radioactive beams are challenging and the number of cases studied to date is limited [10–15]. The techniques used successfully are the conventional transient-field (TF) method at "low" ion velocities [10,15], recoil in vacuum (RIV) [11,14], and high-velocity transient field (HVTF) [12,13]. Of the available techniques only HVTF is applicable for the high-energy beams produced by fragmentation facilities.

We use the terminology "HVTF" to designate measurements in which a projectile nucleus is excited in a glancing collision on a heavier target; it then scatters forward out of the target into vacuum and is subsequently detected downstream

*Present address: ExtreMe Matter Institute EMMI and Research Division, GSI, Darmstadt, and FIAS Frankfurt Institute for Advanced Studies.

†georgi.georgiev@csnsm.in2p3.fr

‡Present address: IPHC, CNRS/IN2P3, UMR7178, Université de Strasbourg, F-67037 Strasbourg, France.

§Present address: INFN-LNL, Legnaro, Italy.

near the beam axis. Often the beam energy is above the Coulomb barrier for a head-on collision between projectile and target nuclei. In contrast the "conventional" low-velocity TF method is typically performed at energies below (or near) the Coulomb barrier for head-on collisions, and the reaction geometry usually corresponds to backward scattering in the center-of-mass frame.

In all cases, the transient-field technique is based on the strong magnetic fields experienced by ions swiftly moving through ferromagnetic hosts. This field is created by the atomic electrons bound to the ion which create hyperfine fields at the nuclear site. In order to obtain a macroscopic net field, a significant fraction of these electrons must have a preferred spatial orientation. In other words, the electrons bound to the moving ion must be polarized. The magnetic field so created can then be sufficiently strong as to perturb significantly the nuclear state of interest within its lifetime. The strongest hyperfine fields, created by the contact field of the K-shell electrons, have a strength proportional to the Z^3 of the ion (see below). For example, the calculated K-shell contact fields for Zn and Ge are 485 and 596 kTesla, respectively.

The highest probability of having a single K-shell (or $1s$) electron bound to the moving ion occurs when the ion velocity is comparable to the K-shell electron velocity $v_{\rm ion} = v_K = Zv_0$, where $v_0 = c/137$ is the Bohr velocity. Therefore it can be expected that the maximum of the transient magnetic field occurs around $v_{\rm ion} = Zv_0$. Indeed this is what has been observed for light nuclei with atomic numbers between 6 and ~20 (see Ref. [2] and the references therein). At first sight, it might be expected that the transient-field at velocities near $v_{\rm ion} = Zv_0$ might show a Z^3 dependence similar to that of the $1s$ contact field. A much weaker Z dependence is in fact observed, although the transient fields for ions moving at Zv_0 do increase steadily with Z while $Z \lesssim 20$ [2,16]. Based on these experimental observations, the high-velocity transient-field (HVTF) technique was developed [12,13]. For light ions this method provides strong fields and large precessions per unit g factor, that can be used for g-factor measurements on low-intensity fast radioactive ion beams. For example, the precession angle in measurements on radioactive beams with $Z \sim 16$ can be around 200 mrad per unit g factor [12,13,16].

However, for applications of the method to heavier ions, the velocity- and Z-dependence of the polarization process must be reconsidered. During the passage of the fast-moving ions through the host material there are multiple interactions in which electrons are picked up and lost. Somehow the polarization must be transferred to the moving ion from the ferromagnetic host. The polarized electrons in iron are conduction electrons; in gadolinium they occupy the bound outer shell $4f$ orbit. In both cases the velocities of the polarized electrons in the host are much smaller than the K-shell electron velocities for heavy projectile ions. For light ions ($Z < 20$) the degree of polarization for single K-shell electrons has been found to be largely independent on the ion velocity up to $v_{\rm ion} \sim Zv_0$ [2,16–20]. However as Z increases the difference between Zv_0 and the velocity of the polarized electrons increases. It cannot be assumed that the polarization does not change for ions moving at velocities near Zv_0 as Z increases. Indeed the experimental results for high-velocity ^{52}Cr ions ($Z = 24$) [21] indicate that the trend of a steady increase of the transient field with Z and toward $v_{\rm ion} = Zv_0$ does not persist (see also [16]). The behavior of the transient field and its consequences for the general applicability of the HVTF method for higher velocity heavier ions produced at fragmentation facilities was therefore investigated as part of this work.

In Sec. II we will discuss the general considerations for the preparation of the experiment. The experimental details will be presented in Sec. III and the analysis procedure will be outlined in Sec. IV. The experimental results will be discussed in Sec. V both from nuclear structure perspective and the general applicability of the HVTF technique to high-velocity ($v_{\rm ion} \sim Zv_0$) and high atomic number ($Z > 30$) radioactive ion beams.

II. EXPERIMENTAL DESIGN

As noted above, the HVTF technique is the only method that can be used on radioactive nuclei produced at fragmentation facilities to measure the g factors of excited states with lifetimes in the picosecond range. The only previous radioactive beam measurement by this method, on ^{38}S and ^{40}S, was performed at NSCL [12,13]. Similar measurements on stable beams include studies on high velocity ^{32}S, ^{40}Ar, and ^{52}Cr [21–24].

Figure 1 shows a sketch of the experimental setup. The ion beam impinges on a secondary target, which typically consists of two layers. The first layer is a high-Z material which serves to excite the 2_1^+ state of the beam nuclei via intermediate energy Coulomb excitation. It may also serve to slow the beam velocity to the regime near Zv_0 so that the transient field can act in the subsequent ferromagnetic layer of the target. After passing through the second (i.e., ferromagnetic) layer of the target, where it experiences the transient field, the excited beam ion emerges into vacuum. As will be discussed below, a single target layer of gadolinium can serve to both excite the nuclei and provide the ferromagnetic medium. For states with picosecond lifetimes, the excited state of the beam ion

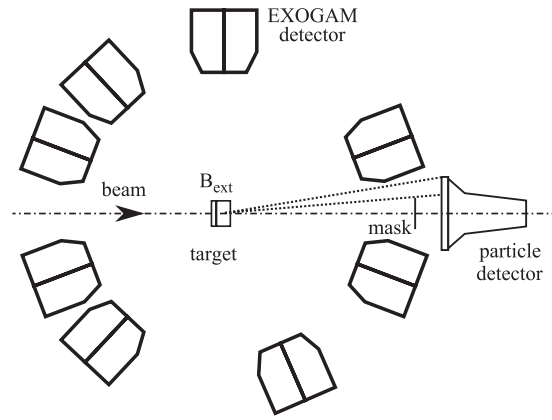

FIG. 1. Experimental setup, from above. The beam traverses the target and is detected in the forward direction. The target is polarized by an external magnetic field $B_{\rm ext}$ directed perpendicular to the page. The de-excitation γ rays are detected by eight EXOGAM detectors.

TABLE I. Excitation energies, $E(2^+)$, reduced transition rates, $B(E2;0^+ \rightarrow 2^+) = B(E2)\uparrow$, and mean lifetimes, $\tau(2^+)$, of 2_1^+ levels.

Nuclide	$E(2^+)$ [keV]	$B(E2)\uparrow$ [e^2fm^4]	$\tau(2^+)$ [ps]
^{76}Ge	563	2680(80)[a]	26.9(8)[a]
^{72}Zn	653	1740(210)[b]	19.8(24)[c]

[a]Reference [32].
[b]Reference [33].
[c]From $B(E2)$ Ref.

decays by γ-ray emission within a few hundred microns after the target. If the ion carries atomic electrons there may be vacuum deorientation effects [25]. The excited beam ions are subsequently detected in the particle detector downstream, in coincidence with γ rays detected by the EXOGAM detectors.

There are competing requirements that the ion must carry electrons inside the ferromagnetic medium in order to generate the transient field, but yet be as free of electrons as possible when it emerges. The velocity of the excited beam ion must be near Zv_0 as it traverses ferromagnetic medium in order to optimize the transient-field precession [16]. At the same time, high charge states (corresponding to no more than a few electrons bound to the ion) are needed to minimize the effect of vacuum deorientation when the ion exits from the target.

The beam energy, target materials, and opening angle of the particle detector should be chosen so that "safe" Coulomb excitation occurs for all events recorded. There will be excitation on the ferromagnetic layer as well as on the target layer, which must be considered when designing the experiment.

Two materials can be considered for use as the ferromagnetic layer, namely iron and gadolinium. Each has advantages and disadvantages. Gadolinium has a lower stopping power than iron, allowing for a longer interaction time of the ion with the transient field. It is also easier to achieve "safe" Coulomb excitation on gadolinium than iron. However, its low Curie temperature (293 K [26]) requires the use of on-line cooling techniques. In contrast, iron is ferromagnetic at room temperature. The higher stopping power in iron can be advantageous when the half-life of the state to be measured is comparable with the interaction time, i.e., for fast beams ($v \approx Zv_0$) and short-lived states with lifetimes of a few picoseconds, as was the case in the measurement on ^{38}S reported in Ref. [12]. In short, the choice of the ferromagnetic material has to be considered carefully case-by-case.

With gadolinium hosts somewhat higher magnetic fields can be reached for light ions [2], however for low-velocity heavier ions the transient fields in iron and gadolinium hosts are usually comparable [27]. Whereas the transient field strength has been measured in gadolinium at Zv_0 for $Z = 24$, there have been no high-velocity calibration measurements on iron hosts for $Z > 14$. Prior to the present experiment there were no experimental data to indicate which host might produce the larger fields for high-velocity $Z \sim 30$ heavy ions. Therefore the TF strengths were measured both in iron and gadolinium hosts with ^{76}Ge beams.

The present experiment was designed by making use of the GKINT code [28], which calculates the kinematics, cross sections and other relevant quantities for the transient-field measurements, based on the theory of intermediate energy Coulomb excitation as developed by Bertulani *et al*. [29,30]. Table I summarizes the relevant properties of the 2_1^+ levels in ^{72}Zn and ^{76}Ge. For ^{76}Ge, $g(2_1^+) = +0.383(20)$ [31] is known with sufficient precision to provide a calibration of the TF strength.

III. EXPERIMENTAL PROCEDURES

The experiment was performed at the GANIL facility using a ^{76}Ge primary beam at 59 MeV/nucleon. Table II gives a summary of the beams, secondary targets and duration of each measurement.

The first measurement (Run I) used a Pb foil without any ferromagnetic layer. The purpose of this rather short run was twofold: First, it was intended to help evaluate the degree of excitation on the iron layer of the target used in Run II, some of which was unsafe and could not be calculated reliably. Second, this measurement gave additional angular correlation data to help evaluate the effects of vacuum deorientation.

In Runs II and III the known g factor of the 2_1^+ state of the ^{76}Ge beam was used to calibrate the strength of the transient field. In order to achieve a velocity range straddling Zv_0 for the ions traversing the iron and gadolinium layers of the targets, and experimental conditions similar to the ^{72}Zn case, the ^{76}Ge energy was degraded down to 38 MeV/nucleon using a 195.5 μm thick Al primary target, and a 553 μm wedge-shaped Be degrader.

TABLE II. Summary of the different runs performed during the experiment.

Run	Beam	Energy [MeV/nucleon]	Target	Thickness [mg/cm^2]	Intensity [pps]	Duration [hours]
I	^{76}Ge	37.8	^{208}Pb	113	6×10^6	1
II	^{76}Ge	37.8	^{208}Pb + Fe + C	91 + 94 + 1	6×10^6	11.5
III	^{76}Ge	37.9	Gd + C	204 + 2	6×10^6	4.5
IV	^{72}Zn	36.5	Gd + C	204 + 2	2.8×10^5	30

The secondary target for Run II consisted of a ^{208}Pb 91 mg/cm^2 layer attached to a ferromagnetic layer of annealed iron 94.3 mg/cm^2 thick. To ensure adhesion, an intermediate layer of 300 μg/cm^2 indium was used, and the foils were pressed together. The 2^+ state of ^{76}Ge was predominantly populated in the Pb layer (≈60% of the total Coulomb excitation). The remaining excitation of the beam took place on the iron layer. A thin layer of carbon on the back of the target was added to help raise the charge state of the ion and hence reduce vacuum deorientation effects (see below).

In Runs III and IV the target was a single-layer of 204 mg/cm^2 Gd, which was used both for the Coulomb excitation of the 2^+ states and as ferromagnetic layer. A thin carbon layer was again added to increase the charge state of the exiting ions. The combination of Coulomb-excitation target and ferromagnetic host by means of a single gadolinium layer can be treated in a straight forward way using the GKINT code. This method has also been used to study high-velocity transient fields acting on Mg ions [34].

The magnetization of the targets was measured off line. These measurements showed that the iron targets can be safely assumed to be fully saturated under the conditions of the experiments. Such thick gadolinium foils have not been used previously for transient-field measurements. Along with the magnetometer measurements, the magnetic behavior of gadolinium foils was therefore also measured in-beam at the Australian National University using 40 MeV ^{16}O beams from the ANU 14UD Pelletron and procedures as described in Ref. [35]. The temperature dependence and sensitivity to the applied field was investigated. From both the in-beam and off-line measurements it was concluded that, under the conditions of the HVTF experiment, the magnetization of the 204 mg/cm^2 gadolinium foil was at least 85% of that routinely achieved in transient-field measurements using thinner foils [35]. Note that a reduced magnetization will reduce the magnitude of the observed transient-field precession, but have no direct consequence for the measurement of the ^{72}Zn g factor relative to that of ^{76}Ge.

Since the precession effect observed with the iron host (Run II) was consistent with zero, despite the relatively high statistics, the gadolinium target was used for the g-factor measurement on ^{72}Zn (Run IV).

Run IV was performed using a radioactive beam of ^{72}Zn. The nuclei of interest were produced by intermediate-energy projectile fragmentation of ^{76}Ge on a 500 μm Be target. The reaction products were separated using the LISE spectrometer [36]. Further purification of the beam was obtained by means of a 416 μm Be wedge degrader. A beam purity of ∼75% was achieved. No beam contaminant lines were visible in the relevant region of the γ-ray spectrum. The beam size on the target was limited by upstream slits to be less than 15 mm, well within the 20 mm separation of the pole tips.

In all of the runs the scattered particles were detected with a plastic scintillator detector covering angles between 3° and 5.5° with respect to the beam axis, measured in the laboratory frame. The particle detector of 140 mm diameter was placed 73 cm down stream of the target to set the maximum scattering angle. Energy, and time of flight as determined relative to the radio frequency of the cyclotron (10.88 MHz), were stored for each particle-γ event.

Direct beam ($\theta < 3°$) was suppressed by placing a mask (90 mm diameter) in front of the particle detector. This angular selection also favored Coulomb excitation over Rutherford scattering [28]. For the ^{72}Zn measurement the count rate in the particle detector was reduced by a factor of about 6, to ∼50 kHz, by use of the mask. The upper limit of the angular coverage of the particle detector (5.5°) was chosen in order to select events of "safe" Coulomb excitation, avoiding impact parameters at which nuclear interactions between the beam and the target nuclei can occur. (The grazing angle at the front of the gadolinium layer is about 5.6° for the ^{76}Ge beam, and a little higher for ^{72}Zn.) Since the particle-γ angular correlation, $W(\theta)$, can be calculated by first principles in Coulomb excitation, with the exception only of the recoil in vacuum (RIV) component, selecting "safe" Coulomb excitation events helps reduce experimental uncertainties in the determination of the particle-γ angular correlation.

Eight EXOGAM detectors [37] were used to detect the γ radiation from the de-excitation of the states of interest (see Fig. 1). Each EXOGAM detector is composed of four HPGe crystals with a fourfold segmentation. This gives enhanced angular granularity and reduces significantly the Doppler broadening. The detectors were positioned in the horizontal plane at distances of 24.5 cm from the target position. The total photo peak efficiency of the setup was estimated to be $\varepsilon_\gamma \approx$ 4.0% at 1332 keV. Six detectors were placed at angles with the highest sensitivity to the precession effect (±26°, ±127°, and ±154°) while the two remaining detectors (positioned at +90° and −60°) were included to obtain a better measurement of the angular correlation of the emitted radiation. In both the angular correlation and precession measurements, the clover elements were exploited such that each clover was split into two detectors at $(\theta \pm 6.5)°$. The data acquisition was triggered by particle-γ coincidences.

Because the radioactive beam was not stopped in the target, but 73 cm downstream, there was practically no buildup of activity in the view of the γ-ray detectors.

The ferromagnetic foils were polarized with an electromagnet providing ≈0.1 T in the vertical direction. The polarity of the field was reversed every 200 s to minimize systematic errors. The direction of the magnetic field, designated "field-up" or "field-down" was written in the event data. The measurement on the iron-backed target (Run II) was performed at room temperature. In Runs III and IV the Gd target was cooled well below its Curie temperature by means of liquid nitrogen.

IV. ANALYSIS PROCEDURES AND RESULTS

Doppler corrected γ-ray spectra corresponding to particle-γ coincidences were constructed from the event data for each direction of the polarizing field. Particle-γ angular correlations were determined from the sum of "field-up" and "field-down" data. Precession effects were determined from double ratios of "field-up" and "field-down" counts in the complementary pairs of detectors according to the standard procedures [2,38].

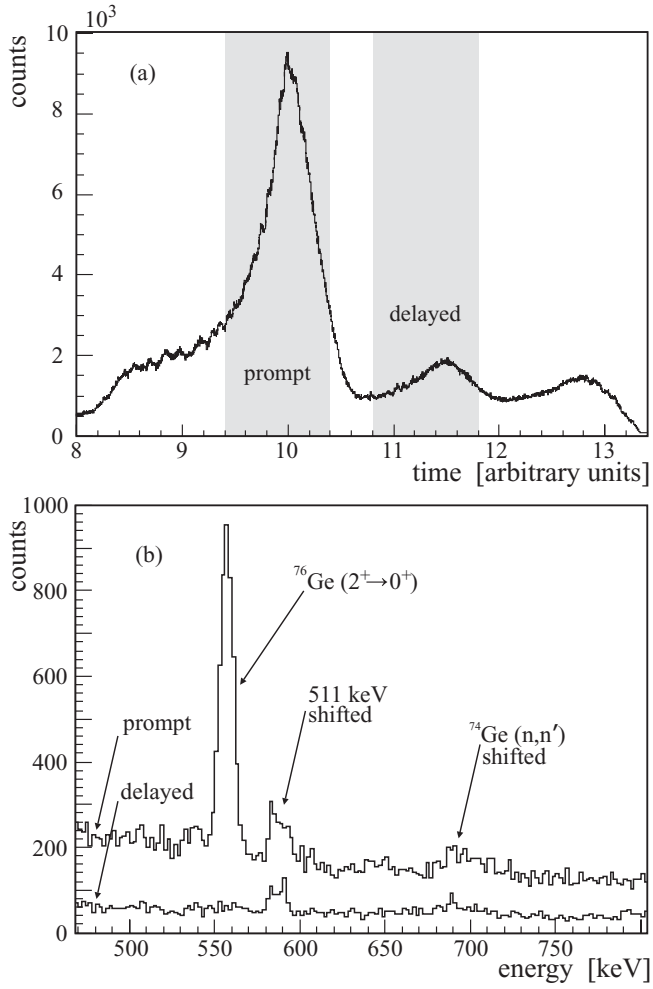

FIG. 2. (a) Total time spectrum for all the detectors in Run III. The two gray zones denote the conditions used for the random event subtraction. The delayed region was chosen to represent an equivalent time interval containing a beam burst. b) "Prompt" and "delayed" Doppler-corrected γ-ray spectra near the ^{76}Ge ($2^+ \rightarrow 0^+$) line. This spectrum represents all of the data for the pair of Clover crystals at 148° with respect to the beam axis in Run III. The "random subtracted spectrum", from which the photopeak intensity is measured, is obtained with the "delayed" spectrum subtracted from the "prompt" one.

Random event subtraction was performed using the prompt and delayed condition on the time spectra (see Fig. 2). This removed the long-lived activities from the γ-ray spectra. A significant reduction of the prompt background was achieved by also requiring a γ-ray multiplicity of one.

In Fig. 3 a typical Doppler-corrected random-subtracted spectrum for Run IV is shown. Note that the particle-γ coincidence condition and random subtraction has strongly suppressed the annihilation radiation and (n, n') events in the Ge detectors.

A summary of the energies and velocities of the Coulomb-excited beam ions as they traversed the ferromagnetic layer of each target is given in Table III. The mean velocity of the ions leaving the target was deduced from the average of the Doppler shifts observed in the segments of both forward and backward

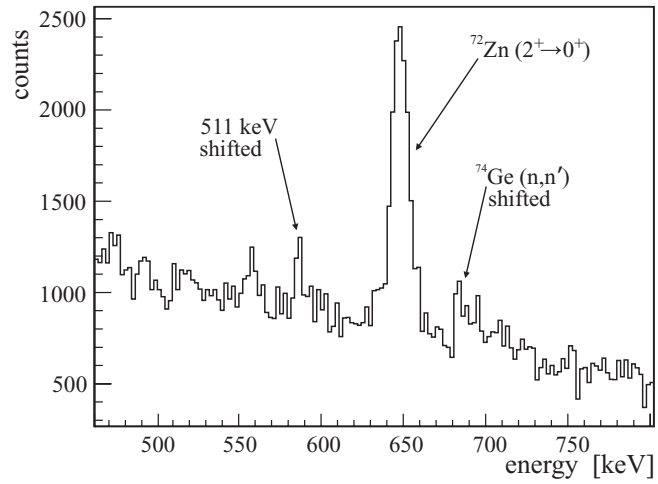

FIG. 3. Doppler-corrected random-subtracted γ-ray spectrum near the ^{72}Zn ($2^+ \rightarrow 0^+$) line. This spectrum represents all of the data for the pair of clover crystals at 148° with respect to the beam axis in Run IV.

detectors. In calculating the kinematic quantities in Table III, the stopping powers were scaled to reproduce the observed exit velocities as determined from the Doppler shifts. In this way it was found that, compared to the stopping powers of Ziegler *et al.* [39], the stopping power for Zn and Ge in Gd was reduced by 3.5%, whereas the stopping power of the iron host was about 10% higher.

A. Angular correlations and vacuum deorientation

The particle-γ angular correlation in the rest frame of the nucleus for the present case of a multipolarity-2 transition and axial symmetry can be written as

$$W_{\rm nuc}(\theta_{\rm nuc}) = 1 + A_2 P_2(\cos\theta_{\rm nuc}) + A_4 P_4(\cos\theta_{\rm nuc}), \quad (1)$$

where $A_k = a_k Q_k G_k, k = 2, 4$, with a_k the angular correlation coefficients calculated with the program GKINT [28] for the case where there is no vacuum deorientation, and point γ-ray detectors. Q_k are the attenuation coefficients to correct for the finite size of the detectors, and G_k are the vacuum attenuation coefficients. Typical a_k values for all of the measurements reported here are $a_2 \simeq -0.6$ and $a_4 \simeq -0.2$. For a single crystal of an EXOGAM clover detector at 24 cm from the target $Q_2 \simeq 0.99$ and $Q_4 \simeq 0.98$. Since $a_4 \sim a_2/3$, the $k = 4$ term has a small effect on the angular correlation.

Obtaining the angular correlations in the laboratory frame, $W_{\rm lab}(\theta_{\rm lab})$, from that in the rest frame of the nucleus, $W_{\rm nuc}(\theta_{\rm nuc})$, or vice versa, requires both transformation of the laboratory angle to the equivalent angle in the rest frame of the nucleus, and a multiplication by the appropriate solid-angle ratio so that the γ-ray flux emitted into 4π is conserved. The relevant expressions have been summarized in Ref. [40], for example.

Examples of laboratory-frame angular correlations from Runs I, III, and IV are shown in Fig. 4. The laboratory-frame data were fitted with G_2 and G_4 as parameters. It was found that the angular correlations are insensitive to the value of G_4. Consequently, the fitted G_2 values are insensitive to any

TABLE III. Kinematic parameters for the recorded particle-γ coincidence events. $E_{i,e}$ and $v_{i,e}/Zv_0$ are the average energy and velocity for Coulomb-excited projectile ions entering and exiting the ferromagnetic layer of the target. ($v_0 = c/137$ is the Bohr velocity.) $\langle v/Zv_0\rangle$ is the average ion velocity in the ferromagnetic layer and $t_{\rm eff}$ is the effective interaction time with the transient field. E_e and v_e/Zv_0 also represent the energy and velocity of the excited ions emerging from the target into vacuum.

Run	Beam:*Host*	E_i [MeV/nucleon]	E_e [MeV/nucleon]	v_i/Zv_0	$\langle v/Zv_0\rangle$	v_e/Zv_0	$t_{\rm eff}$ [ps]
I	^{76}Ge:		25.6			1.00	
II	^{76}Ge:*Fe*	28.9	7.75	1.07	0.83	0.53	1.95
III	^{76}Ge:*Gd*	28.2	12.8	1.05	0.89	0.71	2.18
IV	^{72}Zn:*Gd*	27.2	12.5	1.10	0.94	0.75	2.17

assumed (fixed) value of G_4. For reasons that will be evident in the following, G_4 was set to the value of 0.2 in the fits reported here. It was also found that within experimental uncertainties, the angular correlations for ^{76}Ge in Run III and for ^{72}Zn in Run IV were the same. In other words, the G_2 values extracted from the fits overlapped within experimental uncertainties. Given this experimental result, and the expectation that the angular correlations for these two runs should not differ significantly, the data were combined as shown in Fig. 4.

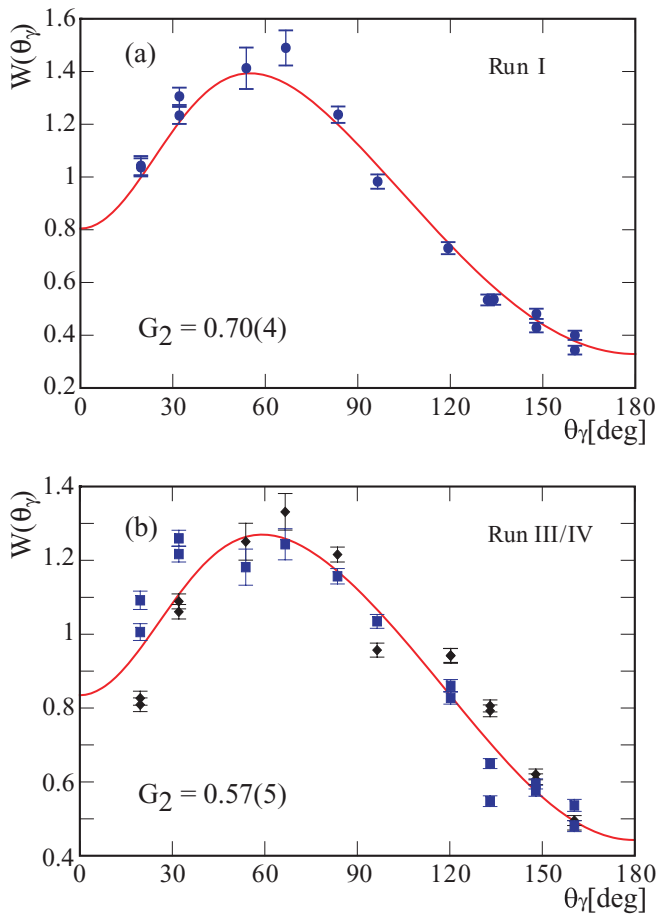

FIG. 4. (Color online) Laboratory frame angular correlations for de-excitation of the first excited state of ^{76}Ge Run I (a) and the combined fit for ^{76}Ge in Run III (b), black diamonds, and ^{72}Zn in Run IV (b), blue squares. Separate points are shown for detectors on each side of the beam axis (see Fig. 1), however the data are combined for the two elements within each clover detector that have the same θ_γ.

The present G_2 values are slightly smaller than the attenuation factors found for H-like ^{52}Cr ions by Grabowy *et al.* [21]. In that work, however, a significant fraction of the ^{52}Cr ions decayed in the target material before entering vacuum, so larger G_k values are to be expected.

Vacuum deorientation has a large impact on the sensitivity of the g-factor measurement, which will be discussed below. The physics of the vacuum deorientation effects, however, will be discussed in more detail here, before proceeding to evaluate the transient-field precessions.

Calculations of the charge-state distributions suggest that ions emerge from the target with up to three electrons in Run I, and with up to four electrons in Runs III and IV. Considering this spread of charge states, schematic calculations of the expected attenuation factors were performed along the lines of the calculations reported by Grabowy *et al.* [21] for ^{52}Cr. As in that work, it can be assumed that the hyperfine frequencies are so high that the attenuation effectively goes immediately to the hard core value. This approximation was valid at $Z = 24$ and is even more justified at $Z = 30$. The hard core attenuation coefficients for electron spins up to $J = 3$ are listed in Table IV. From this table it is evident that for Run I with $G_2 = 0.7$, the average atomic spin is near $J = 1/2$. For Runs III and IV the observed $G_2 \approx 0.6$ corresponds to an average atomic spin between $J = 1/2$ and $J = 1$, being closer to $J = 1/2$. For both cases $G_4 = 0.2$ is a good approximation across the range of G_2 values, as assumed in the fits to the data.

Table V lists the longer-lived electron configurations of few-electron ions that could contribute to the vacuum deorientation. It is evident that if the ions were only in their atomic ground states, the G_2 value would lie between 0.76 and 1. The smaller value observed experimentally indicates that a significant fraction of the ions must have excited configurations with angular momentum reaching up to $J = 2$.

TABLE IV. Hard core vacuum deorientation coefficients.

J	$G_2^{\rm h.c.}$	$G_4^{\rm h.c.}$
0	1	1
1/2	0.760	0.200
1	0.473	0.230
3/2	0.276	0.176
2	0.265	0.156
5/2	0.247	0.143
3	0.235	0.135

TABLE V. Long-lived atomic states in few-electron ions.

Ion	Term ($^{2S+1}L_J$)		
H-like	$^2S_{1/2}$		
He-like	$^1S_0$	$^3S_1$	$^3P_{0,1,2}$
Li-like	$^2S_{1/2}$	$^2P_{1/2,3/2}$	
Be-like	$^1S_0$	$^3P_{0,1,2}$	

The same conclusion was reached in the study on ^{52}Cr, and in related works [21,23]. Our results confirm the expectation that the vacuum deorientation effect can be reduced by limiting the number of electrons bound to the ion as it emerges from the target. The carbon layer on the back of the targets, which is estimated to increase the charge by one, has evidently played a part in limiting the deorientation effect in our measurements.

B. TF precessions

The precession angle $\Delta\theta_{\rm exp}$ was determined using standard analysis techniques [2,38]. For the case where there is a significant Lorentz boost [28,34]

$$\Delta\theta_{\rm exp} = \epsilon_{\rm lab}/S_{\rm nuc},$$

where $S_{\rm nuc}$ is the logarithmic derivative of the angular correlation,

$$S = \frac{1}{W(\theta)}\frac{dW(\theta)}{d\theta}\bigg|_{\theta_\gamma} \tag{2}$$

evaluated at the detection angle θ_γ in the rest frame of the nucleus. The slope S was computed using Eqs. (1) and (2), and with the experimental G_k values determined from fits to the angular correlations. For the clover halves that are sensitive to the precession effect, the average slope was $|S| = 0.61$, with a range from $|S| = 0.54$ to $|S| = 0.66$ at 160° and 148°, respectively.

The counting asymmetry, or "effect", $\epsilon_{\rm lab}$ is determined in the laboratory frame:

$$\epsilon_{\rm lab} = \frac{1-\rho}{1+\rho},$$

where the double ratio ρ is

$$\rho = \sqrt{\frac{N(\theta_\gamma,\uparrow)N(-\theta_\gamma,\downarrow)}{N(-\theta_\gamma,\uparrow)N(\theta_\gamma,\downarrow)}}.$$

ρ is a function only of the number of counts per magnetic field direction (↑ and ↓) at a pair of detection angles $\pm\theta_\gamma$, i.e., it is independent of detector efficiencies and beam current variations throughout the measurement. The average counts per clover-half per field direction was ∼1900 for ^{76}Ge in Run III and ∼2600 for ^{72}Zn in Run IV. By comparison of Figs. 2 and 3 it can be noted that the background level is higher for the radioactive ^{72}Zn beam. The consequence is a larger uncertainty in the precession measurement for ^{72}Zn despite the larger number of counts recorded.

The experimental precession angles $\Delta\theta_{\rm exp}$ are summarized in Table VI. The estimates of the average transient-field strengths in Table VI for ^{76}Ge were obtained with the relation

TABLE VI. Measured precessions, $\Delta\theta_{\rm exp}$, g factors, and transient-field strengths, $\langle B_{\rm tf}\rangle$, for ^{76}Ge and ^{72}Zn ions.

Run	Ion	$\Delta\theta_{\rm exp}$ [mrad]	g	$\langle B_{\rm tf}\rangle$ [kT]
II	^{76}Ge	−6(6)	+0.383(20)[a]	0.17(17)
III	^{76}Ge	−23(11)	+0.383(20)[a]	0.58(28)
IV	^{72}Zn	−16(14)	+0.18(17)[b]	

[a]Reference [31].
[b]Present work.

$$\langle B_{\rm tf}\rangle = -\frac{\hbar}{\mu_N}\frac{\Delta\theta}{g t_{\rm eff}}, \tag{3}$$

where μ_N is the nuclear magneton and $t_{\rm eff}$ is the effective interaction time with the transient field.

C. Transient field calibration and K-shell polarization

The precession angles observed for ^{76}Ge in both iron and gadolinium hosts imply much smaller transient-field strengths than might have been expected based on the data for lower-Z ions. This reduction in field strength must be associated with changes in the effectiveness with which the K-shell electrons, bound to the moving ion, can pick up polarization from the ferromagnetic medium.

For high-velocity ions with $v \sim Zv_0$, the transient-field strength can be written as

$$B_{\rm tf}(v, Z) = p_{1s}q_{1s}(v, Z)B_{1s}(Z), \tag{4}$$

where

$$B_{1s} = 16.7R(Z)Z^3 \ \text{Tesla} \tag{5}$$

is the magnetic field produced at the nucleus by a K-shell (or $1s$) electron and $R(Z) \simeq [1 + (Z/84)^{2.5}]$ is a relativistic correction; q_{1s} is the fraction of ions that carry a single K vacancy, and p_{1s} is the polarization of these vacancies. The velocity dependence of q_{1s} at high velocities is expected to resemble that of the hydrogen-like charge fraction for ions emerging into vacuum, but shifted to a lower energy so that the peak value of $q_{1s} = 0.5$ occurs when $v = Zv_0$. The velocity dependence of q_{1s} can conveniently be parametrized as [16]

$$q_{1s} = \tfrac{1}{2}\sqrt{\rm e}(v/Zv_0)^2{\rm e}^{-\frac{1}{2}(v/Zv_0)^4}. \tag{6}$$

In the present experiments, as well as those discussed below, q_{1s} remains near its maximum value (i.e., between ∼0.37 and 0.5). The following conclusions are therefore not sensitive to the form adopted for q_{1s}. Putting these expressions for B_{1s} and q_{1s} into Eq. (4) suggests that a parametrization of the TF strength at high velocity can be based on

$$B_{\rm tf}(v, Z) = 13.8\ p_{1s}\ Z^3(v/Zv_0)^2{\rm e}^{-\frac{1}{2}(v/Zv_0)^4}\ \text{Tesla}, \tag{7}$$

provided a suitable parametrization of the Z dependence of p_{1s} can be found. In previous work on ions with $Z \leqslant 16$ traversing gadolinium hosts at high velocity it was found that the data could be described by $p_{1s} = (1.94 \pm 0.08)/Z$ [16].

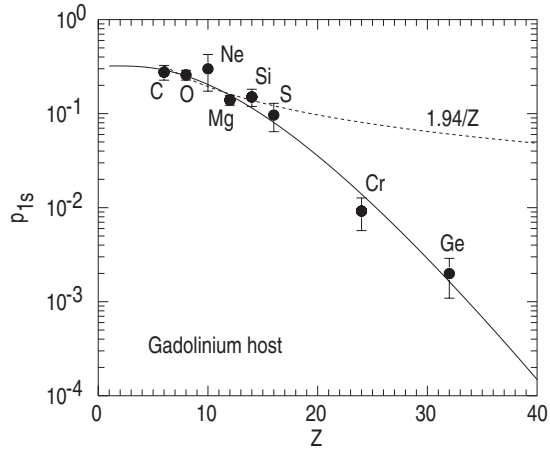

FIG. 5. K-shell polarization in transient-field measurements on ions traversing magnetized gadolinium hosts with velocities near the K-shell electron velocity, Zv_0. The dashed line shows the $1/Z$ dependence which was used previously to describe the low-Z data. The solid curve is the fit to Eq. (8).

This parametrization of p_{1s} fails, however, for the heavier ions studied here.

An extensive series of studies by Speidel and co-workers [21,23,41–44], as summarized in Ref. [16] and supplemented by more recent studies on ^{24}Mg [34], gives experimental transient-field strengths for ions between ^{12}C and ^{52}Cr traversing gadolinium hosts with velocities near Zv_0. These data have been used with the present results, and Eq. (7), to seek a new parametrization of p_{1s} as a function of Z, as shown in Fig. 5.

The solid curve in Fig. 5 is an empirical fit to the function

$$p_{1s} = a \exp[-(\ln Z)^6/b], \tag{8}$$

where the best fit parameters are $a = 0.32(3)$ and $b = 328(25)$. At face value, this procedure assumes that the average value of p_{1s} near Zv_0 does not depend strongly on velocity, but varies with Z. However, because the cases considered are constrained by the requirement that $v \sim Zv_0$, the changes in p_{1s} required to fit the data can equivalently be considered to represent a dependence of p_{1s} on ion velocity.

The data displayed in Fig. 5 do not include corrections for the beam-induced attenuation effects that have been discussed by the Bonn group [2,44]. These effects are negligible for the ions with $Z \lesssim 16$, and are small for the HVTF measurements on ^{72}Zn and ^{76}Ge because of the high beam energies and low beam intensities. The case of ^{52}Cr, however, requires further consideration because a beam attenuation factor of $G_{\text{beam}} = 0.20(6)$ was proposed in Ref. [21]. More recent studies show that this value is too small; an attenuation factor of $G_{\text{beam}} = 0.60(5)$ would now be recommended. Including this factor would raise p_{1s} for Cr from 0.009(4), as plotted in Fig. 5, to 0.015(6). The two values agree within error, and the line of best fit changes very little. The trend seen in Fig. 5 is evidently robust, and our subsequent analysis of the g factor in ^{72}Zn relative to ^{76}Ge is insensitive to any reasonable beam-induced attenuation correction factor which might be applied to the ^{52}Cr data point.

As noted above, in light nuclei, $Z < 20$, the experimentally observed polarization of the $1s$ vacancies in gadolinium hosts was consistent with a $1/Z$ dependence, which is shown by the dashed line in Fig. 5. The magnitude of the polarization for these light nuclei is $p_{1s} \sim 0.1$. The measured precession for ^{76}Ge in gadolinium from the present work implies that the polarization $p_{1s} \sim 0.002$ is about a factor of 50 smaller than found for the lighter ions.

For the iron host, which has been discussed briefly elsewhere [45], the observed field strength of $\langle B_{\text{tf}} \rangle = 0.17(17)$ kTesla implies a K-shell polarization of $p_{1s} = 0.0007(7)$. In discussions of the host dependence of the polarization of K-shell vacancies and the consequent transient-field strength, comparisons are often made with the degree of polarization of the outer shells of the host [19]. For iron, this polarization degree is $2.2/16 = 0.14$, and for gadolinium it is $7.2/36 = 0.20$ [19]. Indeed, larger transient field strengths are observed for light ions traversing gadolinium. In Ref. [16], which focused on light ions, it was suggested that the polarization degree might be falling off faster with increasing Z for gadolinium than for iron hosts, which made it unclear which host would be better for HVTF measurements in the $Z = 30$ region. It is now evident that the transient fields for Ge ions traversing iron hosts at high velocity are 0.4(6) times smaller than the fields for these ions in gadolinium hosts. The experimental uncertainty is too large to draw quantitative conclusions, but it is noteworthy that this experimental polarization ratio is consistent with the ratio of the number of polarized electrons per host atom: $2.2/7.2 = 0.31$.

D. g-factor measurement

The g factor of ^{72}Zn was determined relative to that of ^{76}Ge. Although the experimental conditions were made as near identical as possible, it is evident from Table III that the ions traversed the gadolinium target with slightly different velocities. Moreover, the transient-field strength depends on the Z of the ion, as demonstrated by the K-shell polarization data in Fig. 5. To take into account these differences between the experiments, it is useful to define the precession angle per unit g factor, $\phi = \Delta\theta/g$, in terms of the integral of the transient-field strength:

$$\phi(\tau) = -\frac{\mu_N}{\hbar} \int_{t_i}^{t_e} B_{\text{tf}}(v(t), Z) e^{-t/\tau} dt, \tag{9}$$

where τ is the mean life of the nuclear state, and the transient field strength, $B_{\text{tf}}(v(t), Z)$, depends on the atomic number and velocity of the ion within the ferromagnetic layer of the target. t_i and t_e are the times at which the excited ion enters and leaves the ferromagnetic medium. Equation (9) must be averaged over the excitations taking place throughout the gadolinium target. The computer code GKINT [28] was used to evaluate the average value of $\phi(\tau)$, along with average values of other kinematic quantities such as E_i, E_e, $\langle v/Zv_0 \rangle$, and t_{eff} given in Table III. The computer code evaluates the values of these quantities at each point of Coulomb excitation within the target and weights it by the Coulomb-excitation cross section for that point. The integration is performed over the energy loss of the

beam in the target and the solid angle subtended by the particle detector.

The g factor of ^{72}Zn was determined from

$$g_{\mathrm{Zn}} = \frac{\phi_{\mathrm{Ge}}}{\phi_{\mathrm{Zn}}} \frac{\Delta\theta^{\mathrm{exp}}_{\mathrm{Zn}}}{\Delta\theta^{\mathrm{exp}}_{\mathrm{Ge}}} g_{\mathrm{Ge}}, \tag{10}$$

where $\phi_{\mathrm{Ge}} = 45.4$ mrad and $\phi_{\mathrm{Zn}} = 67.2$ mrad were calculated with GKINT, based on Eqs. (7)–(9). Thus the value we obtain for the g factor of the first 2^+ state in ^{72}Zn is $g = +0.18(17)$. The experimental error is dominated by the uncertainties in the measured precession angles; uncertainties in the velocity and Z dependence of the transient field are negligible in comparison.

V. DISCUSSION

A. Nuclear structure

The physics of the Zn isotopes in the vicinity of ^{68}Ni reveals a complex interplay between the stabilizing effects of the $N = 40$ subshell closure [46–48] and the collective features observed in the Ge isotopes. In order to get deeper insight into the structure of the Zn isotopes, we used several large scale shell model calculations. The results for the g factors of the 2^+ states in the Zn isotopic chain are presented in Fig. 6. Two of the interactions, JJ4B [7] and JUN45 [8], have a core of ^{56}Ni that allows for a reasonable reproduction of the Zn nuclei below $N = 40$. For $N \geqslant 40$ there is a rapid decrease of the experimental $E(2^+)$ energies (see Fig. 7) accompanied by a significant enhancement of experimental $B(E2)$ values, that suggests the development of quadrupole collectivity. These features are not reproduced in the calculations using a ^{56}Ni core due to the missing interactions with the proton $f_{7/2}$ and the neutron $d_{5/2}$ single-particle orbits. A modest reproduction

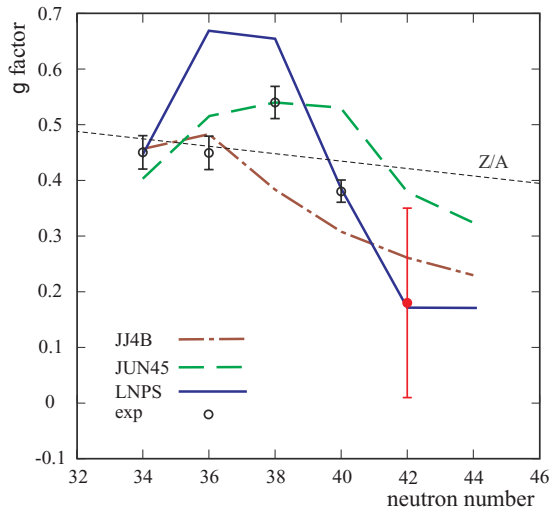

FIG. 6. (Color online) Large scale shell model calculations of the g factors for the first 2^+ state compared to experimental values ([4] and present work) in the zinc isotopic chain. A ^{56}Ni core and effective spin g factors ($g_s^{\mathrm{eff}} = 0.7 g_s^{\mathrm{free}}$) are used in the JJ4B [7] and JUN45 [8] interactions. The possibility of proton excitations is taken into account via the use of a ^{48}Ca core with the LNPS [9] interaction. The effective g factors used by the LNPS interaction are: $g_s^{\mathrm{eff}} = 0.75 g_s^{\mathrm{free}}$, $g_l^{\pi} = 1.1$, $g_l^{\nu} = -0.1$.

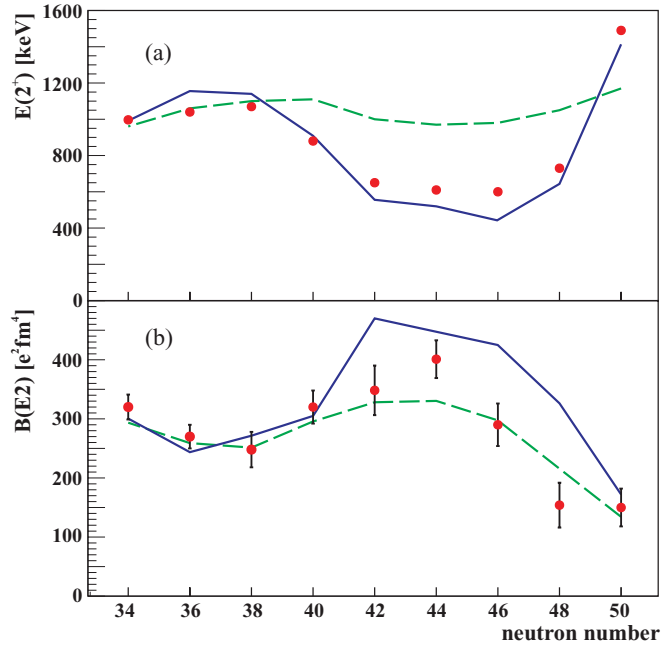

FIG. 7. (Color online) Energies of the 2^+ states (a) and transition probabilities $B(E2; 2^+ \rightarrow 0^+)$ (b) of the Zn isotopes. Filled circles: experiential values, dashed lines: JUN45 interaction [8], solid lines: LNPS interaction [9]. Effective charges of ($e_p = 1.5; e_n = 1.1$) and ($e_p = 1.5; e_n = 0.5$) were used, respectively, for the calculation in the JUN45 and LNPS interactions.

of the $B(E2)$ values in the Zn isotopes is achieved at the cost of a significant boost of the neutron effective charge ($e_n = 1.1$).

A recent interaction (LNPS, Ref. [9]), based on a ^{48}Ca core, takes into account the excitations across the $Z = 28$ shell gap by including the pf-shell orbits for protons and the $1p_{3/2}$, $1p_{1/2}$, $0f_{5/2}$, $0g_{9/2}$, and $1d_{5/2}$ orbits for neutrons. This extended valence space allows various types of excitations to develop and the description of possible coexisting regimes. The interaction was successfully applied to describe the transition from spherical ^{68}Ni to the island of deformation developing around ^{64}Cr. With respect to Ref. [9], a slight modification of the pairing (in particular on the $f_{5/2}$ diagonal matrix element) was made in light of the recent 2^+ energy measurement in ^{80}Zn [49]. These modifications slightly improve the overall spectroscopy of all the nuclei studied around the island of inversion without any significant change in the wave functions. In all of the calculations using the LNPS interaction presented in Figs. 6 and 7 up to ten particle-hole (ph) excitations from $\pi f_{7/2}$ and/or $\nu g_{9/2}$ were allowed.

The agreement between the calculations using the LNPS effective interaction and the data along the zinc isotopic chain is improved for the $E(2^+)$ values, the transition probabilities $B(E2)$ (Fig. 7) and for the g factors as well (Fig. 6). The systematics in the theory reveal a transition occurring at $N = 42$ in ^{72}Zn: the rise of the $(2^+ \rightarrow 0^+)$ $E2$ transition rate appears in conjunction with a sharp decrease of the g factor of the first excited 2_1^+ state. The analysis of the wave function for the ground and first excited states reveals an extra occupancy of two particles in the $g_{9/2}$ and $d_{5/2}$ neutron orbits and almost one particle in the $p_{3/2}$, $f_{5/2}$, and $p_{1/2}$ proton orbits.

The calculations show a transition with increased collectivity toward rotational motion from ^{70}Zn to ^{74}Zn. In the latter, the rotational prescription (see Eqs. (1) and (2) in Ref. [9]) is achieved where one can relate the spectroscopic quadrupole moment and the $B(E2; 2_1^+ \rightarrow 0_1^+)$ to an intrinsic axial shape of $\beta \sim 0.25$. For further insight into the drop starting at $N = 40$ in the systematics of g factors in the zinc isotopic chain, we performed a detailed analysis of proton and neutron contributions: the decrease of the g factors from ^{68}Zn to ^{70}Zn and ^{72}Zn is due to both an increase of the neutron and a slight decrease of the proton contributions. The overestimation of the g factors in ^{66}Zn, ^{68}Zn is probably a sign of the lower convergence of the wave function in these isotopes. The number of ph excitations through the $Z = 28$ and $N = 40$ gaps for those isotopes is greater than for ^{70}Zn and ^{72}Zn due to Pauli blocking effects, leading to a faster convergence of the wave functions for the later. The excellent agreement between the experimental and theoretical energies, reduced transition rates and g factors for ^{70}Zn and ^{72}Zn demonstrates that most of the correlations in those nuclei are already accounted for in the LNPS model space at this truncation level.

B. Evaluation of the HVTF method

The precision of the present measurement was limited by the discovery that the transient-field strength for these higher-Z ions moving with velocities near Zv_0 is considerably weaker than expected based on the transient fields observed at $v \sim Zv_0$ for lighter ions. In fact the average transient field strength achieved for these high velocity ions in gadolinium hosts is about a factor of two smaller than would be achieved for a conventional transient field measurement at an ion velocity of $3v_0$. On the other hand, the net precession angle is still about twice as large as obtained in conventional low-velocity measurements because the interaction time in the HVTF measurements is considerably longer.

The advantage of the HVTF for light ions ($Z < 20$), where precession angles an order of magnitude larger than in conventional low-velocity TF measurements can be achieved, is not as significant for $Z \sim 30$. For measurements of g factors of higher-Z exotic nuclei produced as radioactive beams other techniques like recoil in vacuum and the low-velocity transient field method, should therefore be considered. These techniques require beams with velocities below 5 MeV/nucleon. Although larger precession angles are obtained in HVTF, low-velocity measurements may be advantageous in some cases due to higher radioactive beam intensities, and/or the ability to obtain cleaner γ-ray spectra.

The present measurements were also adversely affected by the attenuation of the angular correlations due to vacuum deorientation. Due to vacuum deorientation with $G_2 \sim 0.6$ and $G_4 \sim 0.2$, the slope of the angular correlation at 30° (lab angle) decreases from an ideal $S \sim 1.65$ to $S \sim 0.65$. A factor of ∼6 increase in statistics is needed to compensate for this reduced slope, compared to the ideal case; for $G_2 \sim 0.7$, the factor by which statistics must be increased falls to 4. (As discussed above, the ideal case of no deorientation cannot be realized in a practical measurement, however it serves here as a reference point.) In the low-velocity regime, the RIV effects can, in principle, be used as a measure of the magnitude of the g factor. Unfortunately at high velocity, the vacuum attenuation effect is practically independent of the g factor and must be avoided as far as possible in the experiments.

For lower-Z ions the HVTF method will remain the method of choice in many cases. The present work demonstrates that the application of the HVTF technique to radioactive nuclei with $Z \lesssim 32$ is feasible for beams with sufficient intensity. Future measurements can be improved by use of a segmented particle detector. This has several advantages. Aside from the trivial advantage that count rate limitations for the particle detector are reduced, the degree of Doppler broadening in the γ-ray spectrum can also be reduced. In the present measurements the effect of opening angle of the particle detector on the Doppler broadening was responsible for the limit on energy resolution that could be achieved. Future use of a segmented particle detector could thus reduce the resulting line widths and hence improve the peak to background ratios. This consideration is of a special importance when performing radioactive-beam measurements in which one typically observes higher background contributions.

The viability and possible application of the HVTF technique to measurements on ions with atomic number considerably higher than $Z = 30$ requires further investigation. The implication of the trend in K-shell polarization shown in Fig. 5 is that the transient-field strengths may become negligibly small, however further experimental data should be obtained before that conclusion is embraced.

VI. CONCLUSIONS

Prior to our experiment, the only other application of the HVTF technique to radioactive beams had been performed at MSU on ^{38,40}S, using an Au-Fe target [12,13]. In the experiment reported here the beam was considerably heavier and the behavior of the transient-field strength was unknown. It was found that the transient-field strength in gadolinium hosts is smaller than might have been expected based on the behavior of lower-Z ions. The transient field for high-velocity Ge in iron was even smaller. Although these overall trends have been revealed, a full characterization of the transient field for high-velocity heavy ions will require further work.

Despite the fact that the precession angle was smaller than hoped, the HVTF technique still achieves larger precession angles than can be achieved in the standard lower-velocity regime. More specifically, the precession angle observed for high velocity ^{76}Ge in gadolinium was about a factor of two larger than is typically obtained in low-velocity transient-field measurements employing projectile excitation and inverse kinematics (see, e.g., [4]). Our work therefore shows that the HVTF technique has advantages for use with radioactive beams produced as intermediate-energy heavy-ion fragments with atomic numbers up to $Z \sim 30$, and beam intensities of the order of 10^5 particles per second and higher. Apart from improving the precision by longer running times, possible directions to improve sensitivity in future measurements include (i) taking steps to limit the effects of vacuum deorientation, and (ii) using a segmented particle detector,

which allows higher beam intensities and improves the slope of the angular correlation.

The results from the g-factor measurement on the radioactive ^{72}Zn hint at the theoretically predicted transition in the structure of the Zn isotopes near $N = 40$.

ACKNOWLEDGMENTS

We thank the GANIL staff for providing the beam and for their assistance throughout the experiment. This work was supported by the EU FP6 contract no. EURONS N° RII3-CT-2004-506065, by the IAP Program, P6/23 BriX, Belgian Science Policy, by the Bulgarian Science Fund DID-02/16 and DFNR-02/5, by the Spanish Ministerio de Ciencia e Innovación under contract nos. FPA2007-66069 and FPA2009-13377-C02-02, the Spanish Consolider-Ingenio 2010 Programme CPAN (CSD2007-00042), and by the Australian Research Council Discovery Grant No. DP0773273. The work of E.F. has been supported in part by the ExtreMe Matter Institute EMMI.

[1] M. Hannawald, T. Kautzsch, A. Wöhr, W. Walters, K.-L. Kratz, V. Fedoseyev, V. Mishin, W. Böhmer, B. Pfeiffer, V. Sebastian, Y. Jading, U. Köster, J. Lettry, H. Ravn, and the ISOLDE Collaboration, Phys. Rev. Lett. **82**, 1391 (1999).
[2] K.-H. Speidel, O. Kenn, and F. Nowacki, Prog. Part. Nucl. Phys. **49**, 91 (2002).
[3] D. Mücher, G. Gürdal, K.-H. Speidel, G. Kumbartzki, N. Benczer-Koller, S. Robinson, Y. Sharon, L. Zamick, A. Lisetskiy, R. Casperson, A. Heinz, B. Krieger, J. Leske, P. Maier-Komor, V. Werner, E. Williams, and R. Winkler, Phys. Rev. C **79**, 054310 (2009).
[4] K. Moschner, K.-H. Speidel, J. Leske, C. Bauer, C. Bernards, L. Bettermann, M. Honma, T. Möller, P. Maier-Komor, and D. Mücher, Phys. Rev. C **82**, 014301 (2010).
[5] O. Kenn, K.-H. Speidel, R. Ernst, J. Gerber, P. Maier-Komor, and F. Nowacki, Phys. Rev. C **63**, 064306 (2001).
[6] N. Stone, At. Data Nucl. Data Tables **90**, 75 (2005).
[7] A. F. Lisetskiy, B. A. Brown, M. Horoi, and H. Grawe, Phys. Rev. C **70**, 044314 (2004); A. F. Lisetskiy (private communication).
[8] M. Honma, T. Otsuka, T. Mizusaki, and M. Hjorth-Jensen, Phys. Rev. C **80**, 064323 (2009). M. Honma (private communication).
[9] S. M. Lenzi, F. Nowacki, A. Poves, and K. Sieja, Phys. Rev. C **82**, 054301 (2010).
[10] G. Kumbartzki, J. R. Cooper, N. Benczer-Koller, K. Hiles, T. J. Mertzimekis, M. J. Taylor, K.-H. Speidel, P. Maier-Komor, L. Bernstein, M. A. McMahan, L. Phair, J. Powell, and D. Wutte, Phys. Lett. B **591**, 213 (2004).
[11] N. J. Stone, A. E. Stuchbery, M. Danchev, J. Pavan, C. L. Timlin, C. Baktash, C. Barton, J. Beene, N. Benczer-Koller, C. R. Bingham, J. Dupak, A. Galindo-Uribarri, C. J. Gross, G. Kumbartzki, D. C. Radford, J. R. Stone, and N. V. Zamfir, Phys. Rev. Lett. **94**, 192501 (2005).
[12] A. D. Davies, A. E. Stuchbery, P. F. Mantica, P. M. Davidson, A. N. Wilson, A. Becerril, B. A. Brown, C. M. Campbell, J. M. Cook, D. C. Dinca, A. Gade, S. N. Liddick, T. J. Mertzimekis, W. F. Mueller, J. R. Terry, B. E. Tomlin, K. Yoneda, and H. Zwahlen, Phys. Rev. Lett. **96**, 112503 (2006).
[13] A. E. Stuchbery, A. D. Davies, P. F. Mantica, P. M. Davidson, A. N. Wilson, A. Becerril, B. A. Brown, C. M. Campbell, J. M. Cook, D. C. Dinca, A. Gade, S. N. Liddick, T. J. Mertzimekis, W. F. Mueller, J. R. Terry, B. E. Tomlin, K. Yoneda, and H. Zwahlen, Phys. Rev. C **74**, 054307 (2006).
[14] A. E. Stuchbery and N. J. Stone, Phys. Rev. C **76**, 034307 (2007).
[15] N. Benczer-Koller, G. Kumbartzki, G. Gürdal, C. Gross, A. Stuchbery, B. Krieger, R. Hatarik, P. O'Malley, S. Pain, L. Segen, C. Baktash, J. Beene, D. Radford, C. Yu, N. Stone, J. Stone, C. Bingham, M. Danchev, R. Grzywacz, and C. Mazzocchi, Phys. Lett. B **664**, 241 (2008).
[16] A. E. Stuchbery, Phys. Rev. C **69**, 064311 (2004).
[17] K.-H. Speidel, Hyperfine Interact. **80**, 1205 (1993).
[18] K. Dybdal, J. Forster, and N. Rud, Nucl. Instrum. Methods **170**, 233 (1980).
[19] N. Rud and K. Dybdal, Phys. Scr. **34**, 561 (1986).
[20] F. Hagelberg, T. P. Das, and K.-H. Speidel, Phys. Rev. C **48**, 2230 (1993).
[21] U. Grabowy, K.-H. Speidel, J. Cub, H. Busch, H.-J. Wollersheim, G. Jakob, A. Gohla, J. Gerber, and M. Loewe, Z. Phys. A **359**, 377 (1997).
[22] H. J. Simonis, F. Hagelberg, M. Knopp, K.-H. Speidel, W. Karle, and J. Gerber, Z. Phys. D **7**, 233 (1987).
[23] J. Cub, M. Bussas, K.-H. Speidel, W. Karle, U. Knopp, H. Busch, H. J. Wollersheim, J. Gerl, K. Vetter, C. Ender, F. Köck, J. Gerber, and F. Hagelberg, Z. Phys. A **345**, 1 (1993).
[24] J. Cub, U. Knopp, K.-H. Speidel, H. Busch, S. Kremeyer, H. J. Wollersheim, N. Martin, X. Hong, K. Vetter, N. Gollwitzer, A. I. Levon, and A. Booten, Nucl. Phys. A **549**, 304 (1992).
[25] G. Goldring, in *Heavy Ion Collisions*, edited by R. Bock (North-Holland, 1982), Vol. 3, p. 483.
[26] H. E. Nigh, S. Legvold, and F. H. Spedding, Phys. Rev. **132**, 1092 (1963).
[27] N. Benczer-Koller and G. J. Kumbartzki, J. Phys. G: Nucl. Part. Phys. **34**, R321 (2007).
[28] A. E. Stuchbery, "Some notes on the program GKINT: Transient-field g-factor kinematics at intermediate energies", (2006), arXiv:nucl-ex/0609032v1.
[29] C. A. Bertulani, A. E. Stuchbery, T. J. Mertzimekis, and A. D. Davies, Phys. Rev. C **68**, 044609 (2003).
[30] A. N. F. Aleixo and C. A. Bertulani, Nucl. Phys. A **505**, 448 (1989).
[31] T. J. Mertzimekis, A. E. Stuchbery, N. Benczer-Koller, and M. J. Taylor, Phys. Rev. C **68**, 054304 (2003).
[32] S. Raman, C. W. Nestor Jr., and P. Tikkanen, At. Data Nucl. Data Tables **78**, 1 (2001).
[33] S. Leenhardt, O. Sorlin, M. G. Porquet, F. Azaiez, J. C. Angelique, M. Belleguic, C. Borcea, C. Bourgeois, J. M. Daugas, C. Donzaud, I. Deloncle, J. Duprat, A. Gillibert, S. Grevy, D. Guillemaud-Mueller, J. Kiener, M. Lewitowicz, S. M. Lukyanov, F. Marie, N. A. Orr, Y.-E. Penionzhkevich, F. de Oliveira Santos, F. Pougheon, M. G. Saint-Laurent,

W. Shuying, Y. Sobolev, and J. S. Winfield, Eur. Phys. J. A **14**, 1 (2002).

[34] A. Stuchbery, A. Wilson, P. Davidson, A. Davies, T. Mertzimekis, S. Liddick, B. Tomlin, and P. Mantica, Phys. Lett. B **611**, 81 (2005).

[35] A. Stuchbery, A. Wilson, P. Davidson, and N. Benczer-Koller, Nucl. Instrum. Methods Phys. Res. B **252**, 230 (2006).

[36] R. Anne, D. Bazin, A. Mueller, J. Jacmart, and M. Langevin, Nucl. Instrum. Methods Phys. Res. A **257**, 215 (1987).

[37] F. Azaiez, Nucl. Phys. A **654**, 1003c (1999).

[38] N. Benczer-Koller, M. Hass, and J. Sak, Annu. Rev. Nucl. Part. Sci. **30**, 53 (1980).

[39] J. Ziegler, J. Biersack, and U. Littmark, *The Stopping and Range of Ions in Solids* (Pergamon, New York, 1985), p. 1.

[40] A. E. Stuchbery, Nucl. Phys. A **723**, 69 (2003).

[41] K. H. Speidel, M. Knopp, W. Karle, M. Mayr, F. Hagelberg, H. J. Simonis, J. Gerber, and P. N. Tandon, Z. Phys. D **6**, 43 (1987).

[42] K.-H. Speidel, F. Hagelberg, M. Knopp, W. Trlenberg, H. Neuburger, J. Gerber, S. S. Hanna, H. Dekhissi, and P. N. Tandon, Z. Phys. D **1**, 363 (1986).

[43] K.-H. Speidel, J. Cub, U. Reuter, F. Passek, H. J. Wollersheim, N. Martin, P. Egelhof, H. Emling, W. Henning, R. S. Simon, R. Schmidt, H. J. Simonis, and N. Gollwitzer, Z. Phys. A **339**, 265 (1991).

[44] K.-H. Speidel, M. Knopp, W. Karle, M. L. Dong, J. Cub, U. Reuter, H. J. Simonis, P. N. Tandon, and J. Gerber, Phys. Lett. B **227**, 16 (1989).

[45] E. Fiori, G. Georgiev, A. E. Stuchbery, A. Jungclaus, D. L. Balabanski, A. Blazhev, S. Cabaret, E. Clement, M. Danchev, J. M. Daugas, S. Grevy, M. Hass, V. Kumar, J. Leske, R. Lozeva, S. Lukyanov, T. J. Mertzimekis, V. Modamio, B. Mouginot, Y. E. Penionzhkevich, L. Perrot, N. Pietralla, K.-H. Speidel, I. Stefan, C. Stodel, J. C. Thomas, and J. Walker, *Nuclear Structure and Dynamics '09: Proceedings of the International Conference*, Vol. 1165 (AIP, New York, 2009), pp. 120–121.

[46] O. Sorlin, S. Leenhardt, C. Donzaud, J. Duprat, F. Azaiez, F. Nowacki, H. Grawe, Z. Dombrádi, F. Amorini, A. Astier, D. Baiborodin, M. Belleguic, C. Borcea, C. Bourgeois, D. M. Cullen, Z. Dlouhy, E. Dragulescu, M. Górska, S. Grévy, D. Guillemaud-Mueller, G. Hagemann, B. Herskind, J. Kiener, R. Lemmon, M. Lewitowicz, S. M. Lukyanov, and P. Mayet, Phys. Rev. Lett. **88**, 092501 (2002).

[47] J. M. Daugas, T. Faul, H. Grawe, M. Pfützner, R. Grzywacz, M. Lewitowicz, N. L. Achouri, J. C. Angélique, D. Baiborodin, R. Bentida, R. Béraud, C. Borcea, C. R. Bingham, W. N. Catford, A. Emsallem, G. de France, K. L. Grzywacz, R. C. Lemmon, M. J. Lopez Jimenez, F. de Oliveira Santos, P. H. Regan, K. Rykaczewski, J. E. Sauvestre, M. Sawicka, M. Stanoiu, K. Sieja, and F. Nowacki, Phys. Rev. C **81**, 034304 (2010).

[48] A. Gade, R. V. F. Janssens, T. Baugher, D. Bazin, B. A. Brown, M. P. Carpenter, C. J. Chiara, A. N. Deacon, S. J. Freeman, G. F. Grinyer, C. R. Hoffman, B. P. Kay, F. G. Kondev, T. Lauritsen, S. McDaniel, K. Meierbachtol, A. Ratkiewicz, S. R. Stroberg, K. A. Walsh, D. Weisshaar, R. Winkler, and S. Zhu, Phys. Rev. C **81**, 051304(R) (2010).

[49] J. Van de Walle, F. Aksouh, F. Ames, T. Behrens, V. Bildstein, A. Blazhev, J. Cederkäll, E. Clément, T. E. Cocolios, T. Davinson, P. Delahaye, J. Eberth, A. Ekström, D. V. Fedorov, V. N. Fedosseev, L. M. Fraile, S. Franchoo, R. Gernhauser, G. Georgiev, D. Habs, K. Heyde, G. Huber, M. Huyse, F. Ibrahim, O. Ivanov, J. Iwanicki, J. Jolie, O. Kester, U. Köster, T. Kröll, R. Krücken, M. Lauer, A. F. Lisetskiy, R. Lutter, B. A. Marsh, P. Mayet, O. Niedermaier, T. Nilsson, M. Pantea, O. Perru, R. Raabe, P. Reiter, M. Sawicka, H. Scheit, G. Schrieder, D. Schwalm, M. D. Seliverstov, T. Sieber, G. Sletten, N. Smirnova, M. Stanoiu, I. Stefanescu, J.-C. Thomas, J. J. Valiente-Dobón, P. Van Duppen, D. Verney, D. Voulot, N. Warr, D. Weisshaar, F. Wenander, B. H. Wolf, and M. Zielińska, Phys. Rev. Lett. **99**, 142501 (2007).